WIND ENERGY
Wind Energ. 2002; **5**:281–300 (DOI: 10.1002/we.66)

Research Article

Multi-flexible-body Dynamic Analysis of Horizontal Axis Wind Turbines

Donghoon Lee, Dewey H. Hodges* and Mayuresh J. Patil,† School of Aerospace Engineering, Georgia Institute of Technology, Atlanta, Georgia 30332-0150, USA

Key words: wind turbine; multi-body dynamics; stability; Floquet analysis; mixed formulation

This article presents a structural dynamic analysis of horizontal axis wind turbines (HAWTs) using a new methodology. The methodology is based on representing a HAWT as a multi-flexible-body system with both rigid- and flexible-body subsystems. The rigid-body subsystems (nacelle, hub) are modelled as interconnected sets of rigid bodies using Kane's method. Kane's method leads to compact equations of motion for rigid-body mechanisms. The flexible-body subsystems (blades, tower) are modelled using geometrically exact, non-linear beam finite elements derived from a mixed variational formulation for the dynamics of moving beams. The use of the mixed formulation allows for the direct determination of constraint forces and moments within the beam finite element and at the boundaries, thus allowing simple connectivity between the finite elements and rigid bodies. The equations for the rigid and flexible subsystems are coupled to obtain a unified framework that models the dynamic behaviour of the complete system. Linearization of the dynamic equations about the steady state solution yields system equations with periodic coefficients that must be solved by Floquet theory to extract the dynamic characteristics. Numerical studies are presented to investigate the natural frequencies and mode shapes for a HAWT with flexible blades and tower.

Introduction

Motivation

The economic costs of electricity generated by wind turbines can be reduced by decreasing construction costs while increasing the wind turbine lifetime and the efficiency of energy conversion. To bring about these improvements, there have been various research efforts throughout the world aimed at better understanding of the wind turbine system. These research efforts encompass various technical disciplines, including atmospheric modelling, wind turbine structural and aerodynamic modelling, energy conversion and power distribution technology. The present effort is directed towards better understanding of the structural dynamic characteristics of wind turbines. It is one of the most important research areas because (1) it leads to accurate prediction of the stress field, which is important for determination of the lifetime, (2) it is a prerequisite for aeroelastic analysis, which is primarily responsible for stability, and (3) it is the basis for control design, which can lead to a significant increase in efficiency.

Previous Work

In the early years of the wind energy industry the effect of structural dynamics was either ignored completely in the design phase or, at best, included through the use of estimated dynamic magnification factors.[1] However,

* Correspondence to: Dewey H. Hodges, School of Aerospace Engineering, Georgia Institute of Technology, Atlanta, Georgia 30332-0150, USA. E-mail: dewey.hodges@ae.gatech.edu
† Department of Mechanical Engineering, Widener University, Chester, Pennsylvania.
Contract/grant sponsor: National Wind Technology Center, NREL; Contract/grant number: XCX-9-29204-03.

Published online 23 August 2002

Received 26 October 2001
Revised 28 March 2002
Accepted 5 April 2002

the flexibility of wind turbine blades and towers has continued to increase to the point where their dynamic behaviour has become quite important.[2]

There have been various advances in structural modelling over the past several decades, and many of these have been assimilated into the various wind turbine design codes. However, the types of structural modelling and analysis found in these codes vary significantly from one another. The structural dynamic analyses found in these codes can be roughly classified into three types of approach: multiple rigid bodies connected by hinges (MBS), finite element method for flexible members (FEM), and the assumed-modes approach. Despite certain differences in implementation, it can be said that MBS is used in ADAMS/WT, DUWECS and FLEXLAST, FEM is used in GAST and TWISTER, and the assumed-modes approach is used in BLADED, FAST-AD, FLEX4, GAROS and VIDYN.[3]

Generally, MBS coupled with a modal solution may be helpful in providing insight into wind turbine modelling at low computational cost. It can also produce a compact system matrix for control design. However, this type of approach is not sufficient for the detailed design of the wind turbines, especially for realistic modelling of rotors with anisotropic blades. On the other hand, FEM may produce quite useful results for these problems, but at high computational cost. Thus FEM has not proven itself to be suitable for preliminary design and performance optimization. Moreover, the final system matrix from FEM is so complicated that it cannot be used for control design. There are some studies that model the horizontal axis wind turbine (HAWT) as a flexible multi-body (see e.g. Reference 4). Most of these studies use numerical computation to find the solutions, which is disadvantageous for the control design of periodic systems. Researchers of the codes have been developing tools to compensate the disadvantages of their codes. However, none of the existing codes is well suited for the cost-effective analysis required at the preliminary design stage, including (1) time domain simulation, (2) analysis of dynamic loads and (3) control design.[3]

Present Work

This article presents a method for structural dynamic modelling and stability analysis of a HAWT based on methodology that was previously proposed by Hodges and Patil.[5] The basic idea of the present work is to model the wind turbine as a multi-flexible-body system with both rigid and flexible subsystems.

The equations of motion for the multi-rigid-body part are derived using Kane's method,[6] which makes it possible to reduce the complexity of those dynamical equations by an appropriate choice of generalized speeds. In the present model the multi-rigid-body part consists of a nacelle, shaft and hub. The nacelle has a yaw degree of freedom with respect to the flexible tower, the shaft rotates with respect to the nacelle with nominal rotor speed, and the hub has a teetering degree of freedom with respect to the shaft. The shaft is presently assumed to be rigid, but shaft torsional flexibility is easily accommodated. A more general representation of shaft flexibility, if needed, will be taken into account in the future. Also, at present the rotor angular speed is assumed to be prescribed. Again, variable rotor speed dependent on the applied wind loads will be included in future models.

The flexible portions consist of the blades and tower. These are represented by mixed, geometrically exact, non-linear beam finite elements derived from the formulation of Reference 7. The beam equations on which this formulation is based can be found in a variety of places (see e.g. References 8–10 and references cited therein) and are based on an extension to dynamics of the static equations of Reissner.[11] The section properties are assumed to be available from a separate analysis such as that of Reference 12. The beam model in its full form accounts for classical deformations (extension, torsion and bending in two directions) and transverse shearing in two directions. It makes use of no small-angle approximations in accounting for the deformation. Unlike the older works cited above, which are displacement formulations, in the present work the equations are put into the weakest form to facilitate the use of the simplest possible shape functions. The use of the mixed formulation allows for the direct determination of constraint forces and moments within the beam finite element and at the boundaries, thus allowing simple connectivity between the finite elements and rigid bodies. By coupling these equations, a set of non-linear ordinary differential equations is obtained. Although the resulting equations are lengthy and complex, these equations are in a form that is simpler than that which could be obtained by other means.

The strategy to solve the derived equations is to separate the solutions into two parts: a non-linear periodic steady state and a transient solution linearized about the periodic steady state. The steady state solution can be calculated either by using the harmonic balance method or by finite elements in time.[13] Linearization about the equilibrium solution yields a set of dynamic equations with periodic coefficients, which must be solved by Floquet theory to obtain the correct modes of the system. To reduce the computational cost, we apply the fast Floquet approach described by Peters.[14]

The previously described model and solution procedure are combined into a single code that can model the flexible part using an arbitrary number of finite elements. The code models the flexible blades and towers as non-uniform, anisotropic, initially curved and twisted beams. Thus twisted and curved rotor blades and realistic tower with varying cross-sectional properties (stiffnesses, mass, etc.) can be modelled. The formulation is general enough to accommodate a rotor with three or more blades, but, to date, the code has been developed only for the two-bladed case. The rigid-body subsystems are modelled using Autolev^{TM}, a symbolic manipulator capable of deriving equations of motion of rigid-body mechanisms using Kane's method. Equations for the flexible portions of the model (blades and tower) are incorporated using the Symbolic Toolbox of MATLAB. By using programming languages that support symbolic computation, the set of symbolic equations of motions can be derived for the complete system, and the symbolic system matrix can be obtained. The present capabilities of the code are (1) structural dynamic modelling, (2) steady state solution, (3) dynamic stability analysis by Floquet theory, (4) analysis of dynamic loads and (5) construction of the dynamic system matrix, potentially useful for control design.

The present analysis is ideally suited for wind turbine analysis. Firstly, as stated above, it can analyze realistic composite blades with initial twist and curvature. The beam model requires accurate cross-sectional stiffness and inertia coefficients, which can be calculated using VABS (variational asymptotic beam sectional analysis).[12] The method was validated by the successful results of several previous works, in which the mixed formulation and VABS are combined for various models.[15,16] Secondly, it can easily accommodate an aerodynamic model. Theoretically, the aerodynamic forces depend on the state variables of the system, and these are directly available in the present formulation. The aerodynamic flow through the wind turbines is modelled using the finite state dynamic inflow model of Peters *et al*.[17] The coupling of the aerodynamic model with the mixed finite element method was validated for the aeroelastic analysis of rotorcraft.[18] Finally, it is possible to use the present framework to treat the dynamic and (in the future) aeroelastic behaviour as well as the control design for the whole wind turbine using symbolic tools.

The symbolic model resulting from the present formulation is one of the most important contributions of the present study. Figure 1 shows the advantage of the present framework over other methodologies for the control design. The first methodology presented in the figure represents a code with rigid-body modelling. Using this methodology, the symbolic system matrix can be obtained, but the accuracy of the solution may not be sufficient to obtain a realistic model, especially for realistic composite blades. The second methodology represents a code with numerical FEM modelling. The results of the code would be very accurate, but it is not possible to represent the system as a symbolic time domain model amenable to preliminary design or control synthesis. Thus the model of the system can be regarded as a black box, which produces only time history responses to inputs. The last methodology in the figure represents the present approach to multi-flexible-body modelling. Using the present framework, one can obtain a symbolic system matrix similar to that obtained in rigid-body modelling while maintaining an accuracy close to that of numerical FEM modelling.

Unfortunately, for a complete aeroelastic analysis the computational costs to derive a symbolic system matrix could increase considerably. Although a state space aerodynamic model is used, it lacks the sparsity present in the structural dynamic equations. Thus symbolic computation for the structural modelling may have to be confined to expressing the boundary forces and moments in terms of other state variables. Moreover, for complex HAWTs it is expected that obtaining the symbolic matrix will become prohibitively expensive as well. For this reason the methodology does have limitations on the complexity of the model.

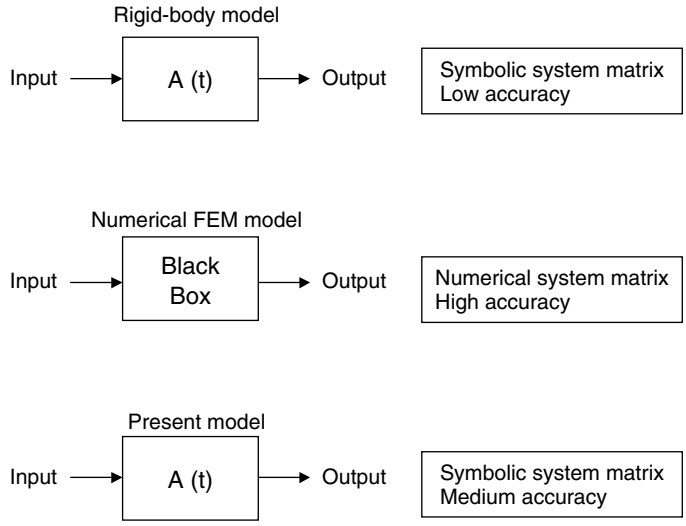

Figure 1. Advantage of the present frame-work

Theoretical Basis

Treatment of Flexible Subsystem

All flexible elements are represented as beams using mixed finite elements. The theoretical details were presented earlier in Reference 5. Here we recapitulate the important steps in the derivation of the equations for the sake of completeness.

We start with the weakest variational formulation given in equation (74) of Reference 7. The weakest form refers to a system description based on the extended Hamilton principle that contains no spatial or temporal derivatives of any unknowns. This weak form is integrated by parts in time and the time integration is removed from virtual quantities as shown in Reference 7. In this way, only the spatial dependence is accounted for in the finite element modelling. The weak form then reduces to

$$\begin{aligned}
&\int_0^\ell \Big\{ [\overline{\delta q}'^T - \overline{\delta q}^T \tilde{\kappa} - \overline{\delta \psi}^T (\tilde{e}_1 + \tilde{\gamma})] F - \overline{\delta q}^T mgB \\
&\quad + \overline{\delta q}^T \dot{P} + (\overline{\delta q}^T \tilde{\Omega} + \overline{\delta \psi}^T \tilde{V})\, P + (\overline{\delta \psi}'^T - \overline{\delta \psi}^T \tilde{\kappa}) M \\
&\quad + \overline{\delta \psi}^T (\dot{H} + \tilde{\Omega} H) + \overline{\delta F}^T [e_1 - C^T (e_1 + \gamma)] \\
&\quad - \overline{\delta F}'^T u - \overline{\delta M}^T (\Delta + \tfrac{1}{2}\tilde{\theta} + \tfrac{1}{4}\theta\theta^T)\kappa - \overline{\delta M}'^T \theta \\
&\quad - \overline{\delta P}^T [v + \tilde{\omega}(x_1 e_1 + u) - C^T V + \dot{u}] \\
&\quad - \overline{\delta H}^T [(\Delta + \tfrac{1}{2}\tilde{\theta} + \tfrac{1}{4}\theta\theta^T)(C\omega - \Omega) + \dot{\theta}] \Big\}\, \mathrm{d}x_1 \\
&\quad = (\overline{\delta q}^T \hat{F} + \overline{\delta \psi}^T \hat{M} - \overline{\delta F}^T \hat{u} - \overline{\delta M}^T \hat{\theta})|_0^\ell
\end{aligned} \tag{1}$$

where u is the column matrix of displacement measures of the beam reference line in the b basis (the undeformed beam cross-sectional frame basis), θ is the column matrix of Rodrigues parameters so that the matrix of direction cosines C, relating the bases of B basis (the deformed beam cross-sectional frame basis) to the b basis, is given by

$$C = \frac{\Delta(1 - \frac{1}{4}\theta^T\theta) - \tilde{\theta} + \frac{1}{2}\theta\theta^T}{1 + \frac{1}{4}\theta^T\theta} \tag{2}$$

F is the column matrix of section force resultant measures in the B basis, M is the column matrix of section moment resultant measures in the B basis, P is the column matrix of section linear momentum measures in the B basis, H is the column matrix of section angular momentum measures in the B basis, γ is the column matrix of force strains, κ is the column matrix of moment strains, V is the column matrix of velocity measures of the beam reference line in the B basis, Ω is the column matrix of cross-sectional angular velocity measures in the B basis, v and ω are the generalized speeds of the body/frame to which the flexible subsystem is attached, mg_B is gravitational force in the B frame, Δ is the 3×3 identity matrix, e_1 is $[1, 0, 0]^T$, $\overline{\delta q}$ is the column matrix of virtual displacement measures in the B basis, $\overline{\delta\psi}$ is the column matrix of virtual rotation measures in the B basis, $\overline{\delta F}$ is the column matrix of virtual force transformed to the b basis, $\overline{\delta M}$ is a column matrix of virtual moment test functions, $\overline{\delta P}$ is the column matrix of virtual linear momentum measures transformed to the b basis, $\overline{\delta H}$ is a column matrix of virtual angular momentum test functions, the overbar of the virtual variables indicates that they are not the variation of a function, all 'hatted' terms on the right-hand side of the equation are the variable values at the boundaries, and all 'primed' and 'dotted' terms represent respectively their spatial and temporal partial derivatives.

The momentum variables (P and H) are related linearly to the velocity variables (V and Ω). When the locus of cross-sectional mass centroids is chosen as the reference line, these relations can be written for an arbitrary cross-section of the beam as

$$\begin{Bmatrix} P \\ H \end{Bmatrix} = \begin{bmatrix} m\Delta & 0 \\ 0 & I \end{bmatrix} \begin{Bmatrix} V \\ \Omega \end{Bmatrix} \tag{3}$$

where m is the mass per unit length of the beam element and I is the moment-of-inertia matrix of the cross-section. By virtue of equation (3), the quantities P and H are eliminated in favour of V and Ω, the 'generalized speeds' of the beam element. Moreover, the force variables (F and M) are related to strain measures (γ and κ) in accordance with the 1D constitutive law as

$$\begin{Bmatrix} F \\ M \end{Bmatrix} = [S] \begin{Bmatrix} \gamma \\ \kappa \end{Bmatrix} \tag{4}$$

where $[S]$ is the cross-sectional stiffness matrix. The stiffness matrix is calculated using VABS and is used to eliminate γ and κ in favour of F and M.

Now the beam is discretized into finite elements. Since the formulation is in its weakest form (spatially), very simple shape functions can be used for the variables. In the present case, none of the variables are differentiated and thus one can use constant shape functions for the variables. Some of the test functions (δ quantities) are spatially differentiated. These test functions can be assumed to be linear within the element. Thus $\overline{\delta q}$ for the ith element can be written as

$$\overline{\delta q} = \overline{\delta q}_i(1 - \eta) + \overline{\delta q}_{i+1}\eta \tag{5}$$

where η is the non-dimensional length co-ordinate within the element. By spatially differentiating the test function, the derivatives of the test functions can be obtained as

$$\overline{\delta q}' = \frac{\overline{\delta q}_{i+1} - \overline{\delta q}_i}{x_\Delta} \tag{6}$$

where x_Δ is the element length.

By collecting terms with various test function coefficients, one can get the set of finite element equations. The whole set of equations for a blade is

$$\overline{\delta q}_1 : -\overline{F}_1 + \frac{x_\Delta}{2}(\dot{\overline{P}}_1 + \tilde{\overline{\Omega}}_1\overline{P}_1 - \tilde{\overline{\kappa}}_1\overline{F}_1 - m\overline{gB}) + \hat{F}_0 = 0$$

$$\overline{\delta q}_i : -\overline{F}_{i+1} + \frac{x_\Delta}{2}(\dot{\overline{P}}_{i+1} + \tilde{\overline{\Omega}}_{i+1}\overline{P}_{i+1} - \tilde{\overline{\kappa}}_{i+1}\overline{F}_{i+1} - m\overline{gB}) + \overline{F}_i + \frac{x_\Delta}{2}(\dot{\overline{P}}_i + \tilde{\overline{\Omega}}_i\overline{P}_i - \tilde{\overline{\kappa}}_i\overline{F}_i - m\overline{gB}) = 0$$

$$\overline{\delta q}_{n+1} : \overline{F}_n + \frac{x_\Delta}{2}(\dot{\overline{P}}_n + \tilde{\overline{\Omega}}_n\overline{P}_n - \tilde{\overline{\kappa}}_n\overline{F}_n - m\overline{gB}) = 0$$

$$
\begin{aligned}
\overline{\delta\psi}_1 &: -\overline{M}_1 + \frac{x_\Delta}{2}[\dot{\overline{H}}_1 + \tilde{\overline{\Omega}}_1\overline{H}_1 - \tilde{\overline{\kappa}}_1\overline{M}_1 - (\tilde{e}_1 + \tilde{\overline{\gamma}}_1)\overline{F}_1] + \hat{M}_0 = 0 \\
\overline{\delta\psi}_i &: -\overline{M}_{i+1} + \frac{x_\Delta}{2}[\dot{\overline{H}}_{i+1} + \tilde{\overline{\Omega}}_{i+1}\overline{H}_{i+1} - \tilde{\overline{\kappa}}_{i+1}\overline{M}_{i+1} - (\tilde{e}_1 + \tilde{\overline{\gamma}}_{i+1})\overline{F}_{i+1}] + \overline{M}_i + \\
&\quad \frac{x_\Delta}{2}[\dot{\overline{H}}_i + \tilde{\overline{\Omega}}_i\overline{H}_i - \tilde{\overline{\kappa}}_i\overline{M}_i - (\tilde{e}_1 + \tilde{\overline{\gamma}}_i)\overline{F}_i] = 0 \\
\overline{\delta\psi}_{n+1} &: \overline{M}_n + \frac{x_\Delta}{2}[\dot{\overline{H}}_n + \tilde{\overline{\Omega}}_n\overline{H}_n - \tilde{\overline{\kappa}}_n\overline{M}_n - (\tilde{e}_1 + \tilde{\overline{\gamma}}_n)\overline{F}_n] = 0 \\
\overline{\delta F}_1 &: \overline{u}_1 + \frac{x_\Delta}{2}[e_1 - \overline{C}_1^T(e_1 + \overline{\gamma}_1)] = 0 \\
\overline{\delta F}_i &: \overline{u}_{i+1} + \frac{x_\Delta}{2}[e_1 - \overline{C}_{i+1}^T(e_1 + \overline{\gamma}_{i+1})] - \overline{u}_i + \frac{x_\Delta}{2}[e_1 - \overline{C}_i^T(e_1 + \overline{\gamma}_i)] = 0 \\
\overline{\delta F}_{n+1} &: -\overline{u}_n + \frac{x_\Delta}{2}[e_1 - \overline{C}_n^T(e_1 + \overline{\gamma}_n)] + \hat{u}_{n+1} = 0 \\
\overline{\delta M}_1 &: \overline{\theta}_1 - \frac{x_\Delta}{2}(\Delta + \tfrac{1}{2}\tilde{\overline{\theta}}_1 + \tfrac{1}{4}\overline{\theta}_1\overline{\theta}_1^T)\kappa_1 = 0 \\
\overline{\delta M}_i &: \overline{\theta}_{i+1} - \frac{x_\Delta}{2}(\Delta + \tfrac{1}{2}\tilde{\overline{\theta}}_{i+1} + \tfrac{1}{4}\overline{\theta}_{i+1}\overline{\theta}_{i+1}^T)\kappa_{i+1} - \overline{\theta}_i - \frac{x_\Delta}{2}(\Delta + \frac{1}{2}\tilde{\overline{\theta}}_i + \tfrac{1}{4}\overline{\theta}_i\overline{\theta}_i^T)\kappa_i = 0 \\
\overline{\delta M}_{n+1} &: -\overline{\theta}_n - \frac{x_\Delta}{2}(\Delta + \tfrac{1}{2}\tilde{\overline{\theta}}_n + \tfrac{1}{4}\overline{\theta}_n\overline{\theta}_n^T)\kappa_n + \hat{\theta}_{n+1} = 0 \\
\overline{\delta P}_i &: \dot{\overline{u}}_i - \overline{C}_i^T\overline{V}_i + v + \tilde{\omega}(\frac{x_i}{2}e_1 + \overline{u}_i) = 0 \\
\overline{\delta H}_i &: \dot{\overline{\theta}}_i - (\Delta + \tfrac{1}{2}\tilde{\overline{\theta}}_i + \tfrac{1}{4}\overline{\theta}_i\overline{\theta}_i^T)(\overline{\Omega}_i - \overline{C}_\omega) = 0
\end{aligned}
\tag{7}
$$

The equations corresponding to $\overline{\delta q_i}$ and $\overline{\delta\psi_i}$ are the discretized equations of motion, the equations corresponding to $\overline{\delta F_i}$ and $\overline{\delta M_i}$ are the discretized strain–displacement relations, and the equations corresponding to $\overline{\delta P_i}$ and $\overline{\delta H_i}$ are the velocity–displacement kinematical equations; the overbar or hat of the variables indicates respectively the element or boundary variables, and the subscripts 1 and $n+1$ of the virtual variables indicate respectively the root and tip of the beam. It should be noted here that, using the above equations, the blade root forces ($\hat{F}_0$) and moments ($\hat{M}_0$) can be written explicitly in terms of the other variables and can be transferred easily to the discrete portion of the system. On the other hand, the v and ω that appear in the kinematical equations are calculated by the rigid-body analysis, as discussed in the next subsection. Also, it is noted that P, H, γ and κ are still used in the above equations to represent the equations more compactly, although they are substituted using V, Ω, F and M in the actual computation.

The above set of equations represents the complete non-linear model required to analyze realistic blades. A similar set of equations can be derived for the tower as well. These equations are quite similar to the above set of equations and are not presented for conciseness.

Treatment of Rigid-body Subsystem

The multi-rigid-body portion of the wind turbine model comprises the collection of rigid bodies. The present model consists of three rigid bodies: the nacelle, shaft and hub. Figure 2 shows the conceptual sketch of the model. However, the number of degrees of freedom for the subsystem is eight, not two, because the tower top displacements and rotations are considered as unknown variables. Otherwise the tower top forces and moments are considered to be given variables derived from the flexible-body analysis of the tower. Frame T, attached to the tower top, can move relative to an inertial frame N restrained only by the stiffness of the tower. Body Y, representing the nacelle, yaws with respect to T about an axis common to both which is parallel to $\mathbf{t}_3 = \mathbf{y}_3$ and passes through a point fixed in both bodies, T_Y. The shaft S rotates with respect to Y about an axis which is parallel to $\mathbf{y}_2 = \mathbf{s}_2$ and passes through Y_s. The motion of the shaft S is prescribed by a constant angular velocity. Body H, representing the hub, teeters with respect to S about an axis which is parallel to $\mathbf{s}_1 = \mathbf{h}_1$ and passes through S_H. Blades are attached to H at points fixed in H.

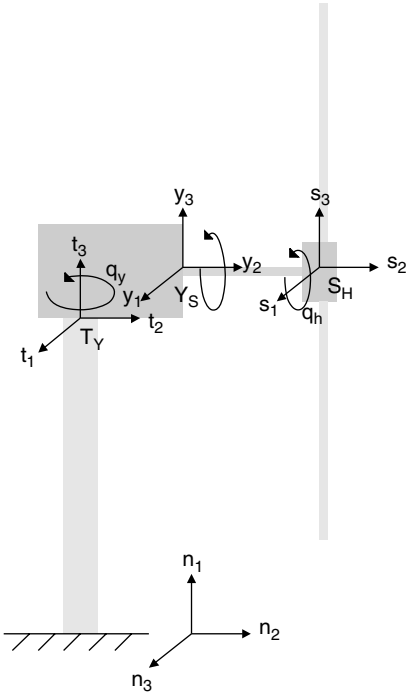

Figure 2. Conceptual model

The generalized co-ordinates for the discrete portion are defined in terms of the yaw angle (q_y) of the body Y with respect to the body T and the teeter angle (q_h) of the body H with respect to the shaft S. The generalized speeds can be defined in various possible ways. Here the definitions of the generalized speeds follow the recommendations of Mitiguy and Kane[19] and are given by

$$\begin{aligned} U_1 &= {}^n\boldsymbol{\omega}^Y \cdot \mathbf{y}_3 \\ U_2 &= {}^n\boldsymbol{\omega}^H \cdot \mathbf{h}_1 \\ [U_3\, U_4\, U_5]^T &= {}^n\boldsymbol{\omega}^T \cdot [\mathbf{t}_1\, \mathbf{t}_2\, \mathbf{t}_3]^T = \left(\frac{\Delta - \tilde{\hat{\theta}}_{n+1}}{1 + \hat{\theta}_{n+1}^T \hat{\theta}_{n+1}/4} \right) \dot{\hat{\theta}}_{n+1} \\ [U_6\, U_7\, U_8]^T &= {}^n\mathbf{v}^T \cdot [\mathbf{t}_1\, \mathbf{t}_2\, \mathbf{t}_3]^T = \hat{C}_{n+1} \dot{\hat{u}}_{n+1} \end{aligned} \tag{8}$$

where the U_i are the generalized speeds and $[U_3\, U_4\, U_5]^T$ and $[U_6\, U_7\, U_8]^T$ represent respectively column matrices of the linear and angular velocity measures for the tower top frame T written in the frame B at the tower top. Using these equations, the time derivative of the generalized co-ordinates can be related to the generalized speeds as

$$\begin{aligned} \dot{q}_y &= U_1 - U_5 \\ \dot{q}_h &= U_2 - (\Omega_0 \mathbf{y}_2 - U_3 \mathbf{t}_1 - U_4 \mathbf{t}_2 - U_1 \mathbf{t}_3) \cdot \mathbf{h}_1 \\ \dot{\hat{\theta}}_{n+1} &= \left(\Delta + \frac{\tilde{\hat{\theta}}_{n+1}}{2} + \frac{\hat{\theta}_{n+1} \hat{\theta}_{n+1}^T}{4} \right) [U_3\, U_4\, U_5]^T \\ \dot{\hat{u}}_{n+1} &= \hat{C}_{n+1}^T [U_6\, U_7\, U_8]^T \end{aligned} \tag{9}$$

It is common for generalized speeds to be taken as measure numbers for the angular velocity of the second body relative to the first. The above definition is thus considerably different. Reference 19 shows that the present type of definition can provide dynamical equations with greatly reduced complexity for the subsystems in which this angular velocity appears. The size of the set of equations of motion derived in the present paper is 70 per cent of one that makes use of the more common definition for the generalized speeds.

Using the above-described choice of generalized speed, one can generate the non-linear, time-dependent equations of motion for the multi-rigid-body subsystem using Autolev. The full non-linear set of equations of motion for the present model is too complex to present here. However, a simplified form equations is presented in Appendix A, after they were linearised about an approximate steady-state solution.

It should be noted that the equations of motion generated by Autolev are dependent on the forces and moments applied to the hub by the blades and to the nacelle by the tower. These forces and moments are calculated by the flexible-blade analysis. The expressions for the velocity (v) and angular velocity (ω) required by the flexible-blade analysis and the tip displacement ($\hat{u}$) and tip rotation ($\hat{\theta}$) required by the flexible-tower analysis are derived by Autolev.

Solution Methodology

Coupling of Subsystems

The two types of subsystem are coupled by transferring the information at the interface between them. In the mixed finite element model for the blades the blade roots are clamped to H at points H_{U_O} and H_{D_O}, and thus the blade root displacement $\hat{u}_0$ and orientation variables $\hat{\theta}_0$ are set equal to zero. The inertial velocity of H_O, the mass center of the hub and angular velocity of H define the motion of the frame to which the blades are clamped and thus determine the variables v and ω needed in the mixed finite element formulation. One can solve for the blade root force $\hat{F}_0$ and moment $\hat{M}_0$ in terms of the element internal variables. This force is applied at the point where the blade is attached to the hub, and the moment is applied to H. Similarly, for the tower the root displacement and rotation are set to zero and the tip displacements and rotations are specified by the rigid-body subsystem. Again, the tower tip force and moment are transferred to the rigid-body subsystem. By accomplishing the above transfer, the two systems are coupled and one obtains the equations of motion for the complete HAWT. The equations can be divided into two parts depending on whether the variables are time differentiated. The complete sets of equations can be represented in a symbolic manner as

$$\mathbf{G}_d(\dot{\mathbf{x}}, \mathbf{x}, \mathbf{y}) = 0, \ \mathbf{G}_a(\mathbf{x}, \mathbf{y}) = 0 \tag{10}$$

where

$$\mathbf{x} = [\mathbf{u}, \boldsymbol{\theta}, \mathbf{V}, \boldsymbol{\Omega}, q_y, q_h, U_1, U_2, \ldots, U_8]^T \tag{11}$$

and

$$\mathbf{y} = [\mathbf{F}, \mathbf{M}]^T \tag{12}$$

with $\mathbf{u}$, $\boldsymbol{\theta}$, $\mathbf{V}$, $\boldsymbol{\Omega}$, $\mathbf{F}$ and $\mathbf{M}$ representing respectively the row matrices containing the set of element values for displacements, Rodrigues parameters, velocities, angular velocities, forces and moments.

Separation of Solutions

The set of equations of motion derived within the flexible-body analysis can be used with a time integration scheme to solve initial value problems. The present framework can be used to solve problems with external forces with minor modifications. One can thus study the non-linear dynamic behaviour of the system by conducting simulations with various initial conditions or external forces.

On the other hand, one could also calculate the non-linear steady state solution and modal characteristics of the system at that steady state. To do so, first the set of non-linear ordinary differential equations is solved by assuming it to be composed of a non-linear steady state solution and a linear transient dynamic one. Mathematically, this can be represented as

$$\mathbf{z} = \mathbf{z}^{SS} + \mathbf{z}^{TS} \tag{13}$$

where

$$\mathbf{z} = [\mathbf{x}, \mathbf{y}]^T \tag{14}$$

Steady State Solution

For simple cases the steady state solution is obvious. For example, for a HAWT with no precone and without consideration of the effects of gravity, the steady state solution is zero for all variables except the axial force and displacement and the velocity and angular velocity components that are non-zero by virtue of the rotor rotation. This approximate solution is easily determined by solving the kinematical equations for the velocity and angular velocity and the simplified steady state equations of motion for the force. For the general case the steady state solution is not only periodic in time but also must be determined from non-linear equations. The calculation of the steady state including gravity is thus quite complicated (and even more so with aerodynamics). There are various methods used to do such analyses, such as harmonic balance, periodic shooting and finite elements in time (over the period). The steady state solution by the harmonic balance method is represented as

$$z^{SS} = h_0 + \sum [h_{cj} \cos(j\Omega t) + h_{sj} \sin(j\Omega t)] \tag{15}$$

This representation of the solution is substituted into the non-linear differential equations of motion to derive the non-linear algebraic equations in terms of the harmonic coefficients. These equations can be solved using a non-linear equation solver to obtain the harmonic coefficients and thus the steady state solution.

Linear Model

If the primary interest is in the modal characteristics, then one needs to linearize the system about the non-linear, periodic, steady state calculated using harmonic balance or some other method. It is noted that the linearization is performed symbolically in the present framework. Linearization about the steady state solutions yields a set of first-order ordinary differential equations with periodic coefficients with the form

$$\begin{aligned} \mathbf{A}\dot{\mathbf{x}} &= \mathbf{B}\mathbf{x} + \mathbf{C}\mathbf{y} \\ 0 &= \mathbf{D}\mathbf{x} + \mathbf{E}\mathbf{y} \end{aligned} \tag{16}$$

where

$$\begin{aligned} A_{ij} &= -\frac{\partial G_{d_i}}{\partial \dot{x}_j} \\ B_{ij} &= \frac{\partial G_{d_i}}{\partial x_j} \\ C_{ij} &= \frac{\partial G_{d_i}}{\partial y_j} \\ D_{ij} &= \frac{\partial G_{a_i}}{\partial x_j} \\ E_{ij} &= \frac{\partial G_{a_i}}{\partial y_j} \end{aligned} \tag{17}$$

Floquet Theory

Owing to the periodic components in the system matrix, Floquet theory is necessary to investigate the modal characteristics of the system. Here the so-called fast Floquet method[14] is used as it saves computer time. In the usual implementation of Floquet theory the linearized periodic system equations are integrated over one period using a set of independent initial conditions equal to the number of states of the system. The state variables at the end of one period help define the Floquet transition matrix. The formula of the fast Floquet method is

$$[\Phi(T, 0)] = ([P][\Phi(\tau, 0)])^Q \tag{18}$$

where $[\Phi(T, 0)]$ is the Floquet transition matrix for a full period, $[P]$ is the permutation matrix, $[\Phi(\tau, 0)]$ is the Floquet transition matrix for $\tau = T/Q$, T is the period and Q is the number of blades.

Here a time-marching scheme is used, based on finite elements in time (a temporal discretization of the above weak form). For the present problem this is equivalent to using a central differencing scheme. The time integration scheme can be represented as

$$\mathbf{A}(\mathrm{t_m})\frac{\mathbf{x}_\mathrm{f} - \mathbf{x}_\mathrm{i}}{\Delta t} = \mathbf{B}(\mathrm{t_m})\frac{\mathbf{x}_\mathrm{f} + \mathbf{x}_\mathrm{i}}{2} + \mathbf{C}(\mathrm{t_m})\mathbf{y}_\mathrm{m}$$
$$0 = \mathbf{D}\frac{\mathbf{x}_\mathrm{f} + \mathbf{x}_\mathrm{i}}{2} + \mathbf{E}\mathbf{y}_\mathrm{m} \tag{19}$$

where $\mathbf{x}_\mathrm{f}$ is the final value of $\mathbf{x}$ for a time step, $\mathbf{x}_\mathrm{i}$ is the initial value of $\mathbf{x}$ for a time step, $\mathbf{y}_\mathrm{m}$ is the constant value of $\mathbf{y}$ for a time step and $\mathrm{t_m}$ is the midpoint of a time step.

The transition matrix provides the modal frequencies and damping. The frequencies are indeterminate by an integer times the rotor angular speed. This indeterminacy can by removed by conducting Fourier analysis on the periodic eigenvector of the system to determine the dominant frequency of the system. To calculate the periodic eigenvector, the system is simulated over a period by using each eigenvector of the Floquet transition matrix as an initial condition. The periodic eigenvector is then derived by representing the time history as a product of the periodic eigenvector and the exponential of the eigenvalue. Now, there are numerous ways of representing this eigenvalue and corresponding periodic eigenvector pair (owing to the eigenvalue uncertainty). It is prudent to transfer the dominant frequency/periodicity to the eigenvalue and keep the eigenvector as close to constant as possible (with some variation due to the possibilities of other frequencies). The dominant frequency of the mode is thus calculated by finding the dominant frequency of the periodic eigenvector (based on an assumed eigenvalue) and then transferring this periodicity from the eigenvector to the eigenvalue. In this way, one represents the mode with an eigenvalue which corresponds to the dominant frequency and an eigenvector denoting the dominant mode shape and presence of other frequencies. The procedure to find dominant eigenvalues is represented by the form

$$\hat{Z}(t) = Z(t)e^{-\lambda t} \tag{20}$$

and

$$\lambda_\mathrm{dom} = \lambda + \max[\mathrm{FFT}(\hat{Z}(t))] \tag{21}$$

where $Z(t)$ is the time history of a state vector with initial conditions given by the eigenvector of $[\Phi(T, 0)]$, λ is the eigenvalue of the Floquet transition matrix normalized by the period, FFT represents the fast Fourier transform function and λ_dom is the dominant eigenvalue.

Results

The methodology described in the previous section is applied to a HAWT model. The rigid-body subsystem degrees of freedom of the model are yaw and teeter. The blades and tower are considered to be flexible in flap bending, lead–lag bending and torsion. The geometric and structural properties of the model are given in Table I. The original source of the table is data from the National Wind Technology Center (NWTC) at the National Renewable Energy Laboratory (NREL), Golden, CO, USA. Some modifications of the original data are undertaken. The geometric parameters are simplified; for example, c_n is zero. Also, the stiffnesses of blades and tower are taken as constant values. The results for a flexible tower are presented in Table II for blades and tower each having two, three and four elements.

The results for the effect of tower flexibility are presented in Table III. The degrees of freedom and the time required for computation increase with an increase in the number of elements, and so does the accuracy. The total number of degrees of freedom for the system is $3M + 6N + 2$, for M elements in the tower and N elements in each blade. The results of dominant frequencies for various tower flexibility values are given in

Table I. Model data

Ω_0	Nominal shaft angular speed	6·02 rad s^{-1}
c_n	Distance from yaw axis to nacelle mass centre	0·0 m
c_s	Distance from yaw axis to shaft mass centre	0·0 m
c_h	Distance from teeter axis to hub mass centre	0·0 m
d_{n_2}	Distance from yaw axis to teeter axis	2·388 m
d_{h_1}	Distance from teeter axis to blade root	0·0 m
d_{h_2}	Distance from shaft axis to blade root	1·8 m
m_y	Mass of nacelle	6900 kg
m_s	Mass of shaft	0·0 kg
m_h	Mass of hub	0·0 kg
I_{y_1}	Moment of inertia of nacelle about lateral axis	0·0 kg m^2
I_{y_2}	Moment of inertia of nacelle about longitudinal axis	0·0 kg m^2
I_{y_3}	Moment of inertia of nacelle about yaw axis	16 599 kg m^2
$I_{s_{\text{lat}}}$	Moment of inertia of shaft about lateral axis	0·0 kg m^2
$I_{s_{\text{long}}}$	Moment of inertia of shaft about longitudinal axis	0·0 kg m^2
I_{h_1}	Moment of inertia of hub about teeter axis	50 kg m^2
I_{h_2}	Moment of inertia of hub about shaft axis	5 kg m^2
I_{h_3}	Moment of inertia of hub about lateral axis	50 kg m^2
K_y	Yaw stiffness	0·0 N m rad^{-1}
C_y	Yaw damper coefficient	0·0 N m s rad^{-1}
K_h	Teeter stiffness	0·0 N m rad^{-1}
C_h	Teeter damper coefficient	0·0 N m s rad^{-1}
l_b	Length of blade	8·42 m
l_t	Length of tower	27 m
m_b	Mass per unit span of a blade	67·5772 kg m^{-1}
m_t	Mass per unit span of tower	67·5772 kg m^{-1}
I_1^b	Cross-sectional moment of inertia of blade for torsion	5 kg m^2 m^{-1}
I_2^b	Cross-sectional moment of inertia of blade for flapping	0·0001 kg m^2 m^{-1}
I_3^b	Cross-sectional moment of inertia of blade for lead–lag	4·9999 kg m^2 m^{-1}
I_1^t	Cross-sectional moment of inertia of tower for torsion	5 kg m^2 m^{-1}
I_2^t	Cross-sectional moment of inertia of tower about lateral axis	0·0001 kg m^2 m^{-1}
I_3^t	Cross-sectional moment of inertia of tower about longitudinal axis	4·9999 kg m^2 m^{-1}
GJ^b	Torsional rigidity of blade	$1{\cdot}0 \times 10^7$ N m^2
EI_2^b	Bending rigidity of blade in flapping motion	$1{\cdot}0 \times 10^7$ N m^2
EI_3^b	Bending rigidity of blade in lead–lag motion	$1{\cdot}0 \times 10^7$ N m^2
GJ^t	Torsional rigidity of tower	$1{\cdot}0 \times 10^9$ N m^2
EI_2^t	Bending rigidity of tower in longitudinal motion	$1{\cdot}0 \times 10^9$ N m^2
EI_3^t	Bending rigidity of tower in lateral motion	$1{\cdot}0 \times 10^9$ N m^2

Table III. The table shows the frequencies for a rigid tower as well as for tower stiffnesses that are 10, 100 and 1000 times that of the blades.

For the present example the first two modes in flap bending, lead–lag bending and torsion are converged by using four elements for the blades and tower. The results use 500 time steps for Floquet theory. It should be noted that the frequencies given in Tables II and III are the dominant frequencies. The response in general contains other frequencies, but in the present example the contributions from the other frequencies are quite small. Some of the blade modes couple strongly with the tower modes and change with tower flexibility, especially the symmetric flapping mode. As the tower stiffness increases, the frequencies of the blade modes converge well to the rigid-tower case.

Figures 3–6 show the first four flap-dominated blade modes. Note that the mode shapes depicted here represent the periodic modes evaluated when the rotor is in the vertical. The symmetric modes couple with the fore–aft bending modes of the tower. This is expected, since the forces and moments transferred to the rigid body (teeter) by the two blades are equal in magnitude and opposite in direction. Here the tower mode shape amplitude is exaggerated so it can be seen in the plots. Also, the antisymmetric modes have a strong coupling with the teetering degree of freedom, as can be seen in the plots. Finally, all modes

Table II. Dominant frequencies of the HAWT with number of elements

Number of elements	Eigenvalues per revolution		
	2	3	4
Yaw	0	0	0
Teeter	$\pm 0{\cdot}009i$	$\pm 0{\cdot}009i$	$\pm 0{\cdot}009i$
1st tower lateral bending	$\pm 0{\cdot}282i$	$\pm 0{\cdot}291i$	$\pm 0{\cdot}292i$
2nd tower lateral bending	$\pm 14{\cdot}711i$	$\pm 8{\cdot}711i$	$\pm 8{\cdot}377i$
1st tower fore–aft bending	$\pm 0{\cdot}930i$	$\pm 0{\cdot}938i$	$\pm 0{\cdot}938i$
2nd tower fore–aft bending	$\pm 11{\cdot}785i$	$\pm 8{\cdot}052i$	$\pm 7{\cdot}615i$
1st tower torsion	$\pm 56{\cdot}940i$	$\pm 56{\cdot}824i$	$\pm 56{\cdot}431i$
2nd tower torsion	$\pm 99{\cdot}990i$	$\pm 98{\cdot}128i$	$\pm 97{\cdot}049i$
1st symm. flap	$\pm 0{\cdot}315i$	$\pm 0{\cdot}317i$	$\pm 0{\cdot}320i$
1st anti-symm. flap	$\pm 3{\cdot}410i$	$\pm 2{\cdot}935i$	$\pm 2{\cdot}624i$
2nd symm. flap	$\pm 8{\cdot}365i$	$\pm 5{\cdot}937i$	$\pm 4{\cdot}710i$
2nd anti-symm. flap	$\pm 23{\cdot}748i$	$\pm 12{\cdot}500i$	$\pm 9{\cdot}583i$
1st symm. torsion	$\pm 15{\cdot}482i$	$\pm 14{\cdot}078i$	$\pm 13{\cdot}936i$
1st anti-symm. torsion	$\pm 14{\cdot}822i$	$\pm 14{\cdot}123i$	$\pm 13{\cdot}935i$
2nd symm. torsion	$\pm 46{\cdot}212i$	$\pm 43{\cdot}471i$	$\pm 41{\cdot}610i$
2nd anti-symm. torsion	$\pm 46{\cdot}233i$	$\pm 43{\cdot}459i$	$\pm 41{\cdot}662i$
1st symm. lead–lag	$\pm 0{\cdot}498i$	$\pm 0{\cdot}490i$	$\pm 0{\cdot}491i$
1st anti-symm. lead–lag	$\pm 0{\cdot}662i$	$\pm 0{\cdot}654i$	$\pm 0{\cdot}655i$
2nd symm. lead–lag	$\pm 7{\cdot}408i$	$\pm 5{\cdot}399i$	$\pm 4{\cdot}465i$
2nd anti-symm. lead–lag	$\pm 7{\cdot}589i$	$\pm 5{\cdot}550i$	$\pm 5{\cdot}345i$

Table III. Dominant frequencies of the HAWT with tower stiffness

Ratio of tower to blade rigidity	Eigenvalues per revolution			
	10	100	1000	∞
Yaw	0	0	0	0
Teeter	$\pm 0{\cdot}009i$	$\pm 0{\cdot}009i$	$\pm 0{\cdot}009i$	$\pm 0{\cdot}009i$
1st tower lateral bending	$\pm 0{\cdot}219i$	$\pm 0{\cdot}292i$	$\pm 0{\cdot}760i$	
2nd tower lateral bending	$\pm 3{\cdot}164i$	$\pm 8{\cdot}377i$	$\pm 22{\cdot}225i$	
1st tower fore–aft bending	$\pm 0{\cdot}920i$	$\pm 0{\cdot}938i$	$\pm 1{\cdot}494i$	
2nd tower fore–aft bending	$\pm 4{\cdot}584i$	$\pm 7{\cdot}615i$	$\pm 23{\cdot}985i$	
1st tower torsion	$\pm 21{\cdot}460i$	$\pm 56{\cdot}431i$	$\pm 148{\cdot}091i$	
2nd tower torsion	$\pm 79{\cdot}450i$	$\pm 97{\cdot}049i$	$\pm 235{\cdot}723i$	
1st symm. flap	$\pm 0{\cdot}217i$	$\pm 0{\cdot}320i$	$\pm 0{\cdot}667i$	$\pm 0{\cdot}802i$
1st anti-symm. flap	$\pm 2{\cdot}624i$	$\pm 2{\cdot}624i$	$\pm 2{\cdot}624i$	$\pm 2{\cdot}624i$
2nd symm. flap	$\pm 4{\cdot}660i$	$\pm 4{\cdot}710i$	$\pm 4{\cdot}737i$	$\pm 5{\cdot}495i$
2nd anti-symm. flap	$\pm 9{\cdot}578i$	$\pm 9{\cdot}583i$	$\pm 9{\cdot}583i$	$\pm 9{\cdot}583i$
1st symm. torsion	$\pm 13{\cdot}937i$	$\pm 13{\cdot}936i$	$\pm 13{\cdot}937i$	$\pm 13{\cdot}937i$
1st anti-symm. torsion	$\pm 14{\cdot}093i$	$\pm 13{\cdot}935i$	$\pm 13{\cdot}947i$	$\pm 13{\cdot}972i$
2nd symm. torsion	$\pm 41{\cdot}610i$	$\pm 41{\cdot}610i$	$\pm 41{\cdot}610i$	$\pm 41{\cdot}610i$
2nd anti-symm. torsion	$\pm 41{\cdot}724i$	$\pm 41{\cdot}662i$	$\pm 41{\cdot}610i$	$\pm 41{\cdot}620i$
1st symm. lead–lag	$\pm 0{\cdot}467i$	$\pm 0{\cdot}491i$	$\pm 0{\cdot}494i$	$\pm 0{\cdot}496i$
1st anti-symm. lead–lag	$\pm 0{\cdot}477i$	$\pm 0{\cdot}655i$	$\pm 0{\cdot}633i$	$\pm 0{\cdot}639i$
2nd symm. lead–lag	$\pm 4{\cdot}223i$	$\pm 4{\cdot}465i$	$\pm 5{\cdot}300i$	$\pm 5{\cdot}356i$
2nd anti-symm. lead–lag	$\pm 4{\cdot}660i$	$\pm 5{\cdot}345i$	$\pm 5{\cdot}647i$	$\pm 5{\cdot}588i$

also have very small contributions from tower lateral bending and torsion and from yaw, not shown in the figures.

Figures 7–10 show the first four torsion-dominated blade modes. Owing to the difficulty in illustrating torsion deformation, the deformation of a straight line on a circular rod undergoing the same twist as the

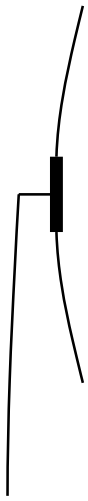

Figure 3. First symmetric flapping mode (0·320)

Figure 4. Second symmetric flapping mode (4·710)

present eigenvector is shown. Here the symmetric modes do not interact with other degrees of freedom. The definition of symmetric/antisymmetric mode needs to be clarified for blade torsion and lead–lag. For flapping, the symmetric mode is simply the mode in which both blades deform in the same manner, out of the plane of rotation in the same direction. On the other hand, for the torsion and lead–lag modes the deformations are in the plane of rotation. Here the symmetric torsion mode is defined to be the one for which both blades experience twist of the same sign in their respective blade frames of reference. Similarly, the symmetric lead–lag mode is defined to be the one for which both blades experience lead–lag deflection of the same sign in their respective blade frames of reference. One sees that the symmetric torsion and lead–lag modes do not interact with other modes, because the forces and moments transferred to the hub are equal and opposite and thus are cancelled. The antisymmetric torsion modes couple weakly with the yaw mode, as expected from the transfer of yawing moment from the blade root via the hub.

Figures 11–14 show the first four lead–lag bending modes of the blades. The symmetric modes are purely lead–lag bending modes. The antisymmetric modes couple with lateral bending modes of the tower, along

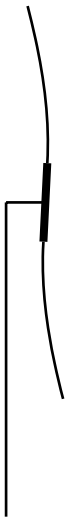

Figure 5. First antisymmetric flapping mode (2·624)

Figure 6. Second antisymmetric flapping mode (9·583)

with the yaw mode, because the inertia force induces forces and moments at the tower top when both blades move in the same direction. It is interesting that the yawing component vibrates at a frequency that is once per revolution greater than the lead–lag motion. This is possibly because the inertial coupling described above is only present when the blades are vertical. When the blades are horizontal, the antisymmetric lead–lag mode would couple inertially with the nacelle pitch degree of freedom, if it were present. Also, the mode shape of the second antisymmetric lead–lag mode couples with the lateral bending of the tower for this model of HAWT.

Conclusion

The article presents a methodology for the dynamic stability analysis of a horizontal axis wind turbine (HAWT) and presents numerical results. The analysis framework is based on separating the complete HAWT system into flexible- and rigid-body subsystems. The equations of motion for the subsystem of rigid bodies

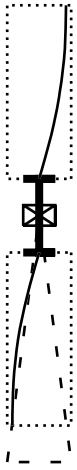

Figure 7. First symmetric torsion mode (13·936)

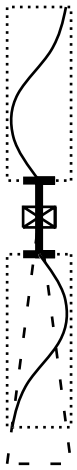

Figure 8. Second symmetric torsion mode (41·610)

are dependent on the boundary conditions from the flexible subsystem (tower and blades); and the frame motion of the blades and tip deflection of the tower come from the rigid-body subsystem. Using the boundary conditions, the equations of motion for the subsystems can be coupled to get the complete system equations. Once the governing equations are linearized about the steady state solution, Floquet theory is then used to extract the characteristic exponents of the complete system.

The numerical results presented in the article are for a two-bladed HAWT with flexible blades and tower. Rigid-body subsystem degrees of freedom include yaw and teeter, whereas the blades and tower are assumed to be flexible in torsion and bending in two directions. The results give the dynamic characteristics of the HAWT, including dominant eigenvalues and mode shapes. A convergence study indicates that four finite elements for each blade are sufficient to calculate the first few modes of the system. Also, a time-marching algorithm based on finite elements in time (equivalent to a central differencing scheme) was found to be simple, efficient and accurate for the time marching required for the application of Floquet theory.

This work will be extended in later articles to include a complete aeroelastic model based on the present structural model and an aerodynamic wake model. The aeroelastic framework will be applied to the aeroelastic analysis of HAWTs with composite blades. The cross-sectional analysis of the composite blades will be

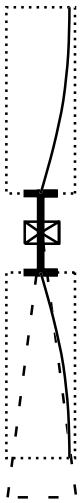

Figure 9. First antisymmetric torsion mode (13·935)

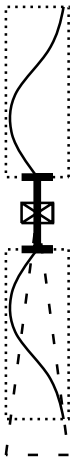

Figure 10. Second antisymmetric torsion mode (41·662)

accomplished using VABS. The aeroelastic framework will be used for time domain simulation, aeroelastic stability characteristics, aeroelastic optimization and, where possible, obtaining a symbolic aeroelastic system matrix for use in control design.

Acknowledgement

This work is sponsored by the National Wind Technology Center, NREL under subcontract XCX-9-29204-03.

Appendix A

$$0 = (d_{h_1} - d_{n_2})\cos(\Omega_0 t)\hat{F}^u_{2_0} + (K_h - c_h d_{n_2} m_h \Omega_0^2)\sin(\Omega_0 t) q_h$$
$$+ (C_h \sin(\Omega_0 t) - \Omega_0 (I_{h_2} - I_{h_1} - I_{h_3} - 2c_h m_h (c_h - d_{n_2}))\cos(\Omega_0 t)) U_2$$

Figure 11. First symmetric lead-lag mode (0.491)

Figure 12. Second symmetric lead-lag mode (4.465)

$$
\begin{aligned}
&+ c_h m_h \sin(\Omega_0 t)\cos(\Omega_0 t)\dot{U}_8 - K_y q_y - \cos(\Omega_0 t)\hat{M}^d_{1_0} - d_{n_2}\sin(\Omega_0 t)\hat{F}^u_{1_0} \\
&- (d_{h_1} - d_{n_2})\cos(\Omega_0 t)\hat{F}^d_{2_0} - (C_y - 2\Omega_0(I_{h_3} c_h m_h (c_h - 1.5 d_{n_2}))\sin(\Omega_0 t)\cos(\Omega_0 t))U_1 \\
&- \Omega_0(I_{s_{\text{long}}} + 2I_{h_3}\cos(\Omega_0 t)^2 + 2c_h m_h (c_h - d_{n_2} - (c_h - 1{\cdot}5 d_{n_2})\sin(\Omega_0 t)^2))U_3 \\
&- c_h d_{n_2} m_h \sin(\Omega_0 t)\dot{U}_2 - (I_{h_3} + c_h m_h (c_h - 2d_{n_2}))\sin(\Omega_0 t)\cos(\Omega_0 t)\dot{U}_3 \\
&- (c_n m_y + c_s m_s - m_h (d_{n_2} - c_h \cos(\Omega_0 t)^2))\dot{U}_6 + d_{n_2}\sin(\Omega_0 t)\hat{F}^d_{1_0}
\end{aligned}
$$

Figure 13. First anti-symmetric lead-lag mode (0.655)

Figure 14. Second anti-symmetric lead-lag mode (5.345)

$$
\begin{aligned}
&- (I_{s_{\text{lat}}} + I_{y_3} m_s c_s^2 + m_y c_n^2 + I_{h_3} \cos(\Omega_0 t)^2 + d_{n_2}(\overline{F}^d_{1_0} - \overline{F}^u_{1_0}) \sin(\Omega_0 t) \\
&- m_h(2 c_h d_{n_2} \cos(\Omega_0 t)^2 - d_{n_2}^2 - c_h^2 \cos(\Omega_0 t)^2))\dot{U}_1 + \cos(\Omega_0 t)\hat{M}^u_{1_0} \\
0 = {} & d_{h_1}(\overline{F}^d_{1_0} - \overline{F}^u_{1_0}) + \hat{M}^u_{2_0} + C_h U_2 + d_{h_1}\hat{F}^d_{1_0} + d_{h_2}\hat{F}^d_{3_0} + (K_h + \Omega_0^2(I_{h_2} - I_{h_3} - m_h c_h^2))q_h \\
&+ \Omega_0(I_{h_2} - I_{h_3} - m_h c_h^2)\sin(\Omega_0 t)U_3 + \Omega_0(I_{h_2} - I_{h_3} - m_h c_h^2)\cos(\Omega_0 t)U_1 \\
&+ c_h m_h \sin(\Omega_0 t)\dot{U}_6 c_h m_h \cos(\Omega_0 t)\dot{U}_8 + c_h d_{n_2} m_h \cos(\Omega_0 t)\dot{U}_3 \\
&- \hat{M}^d_{2_0} - d_{h_1}\hat{F}^u_{1_0} - d_{h_2}\hat{F}^u_{3_0} - (I_{h_1} + m_h c_h^2)\dot{U}_2 - c_h d_{n_2} m_h \sin(\Omega_0 t)\dot{U}_1
\end{aligned}
$$

$$
\begin{aligned}
0 &= \hat{M}^t_{1_l} + \sin(\Omega_0 t)\hat{M}^u_{1_0} + d_{n_2}\cos(\Omega_0 t)\hat{F}^u_{1_0} + (d_{h_1} - d_{n_2})\sin(\Omega_0 t)\hat{F}^u_{2_0} - d_{n_2}\cos(\Omega_0 t)\hat{F}^d_{1_0} \\
&\quad + \Omega_0(I_{s_{\text{long}}} + 2I_{h_3}\sin(\Omega_0 t)^2 + c_h m_h(d_{n_2} + 2(c_h - 1{\cdot}5d_{n_2})\sin(\Omega_0 t)^2))U_1 \\
&\quad + c_h d_{n_2} m_h \cos(\Omega_0 t)\dot{U}_2 + (c_n m_y + c_s m_s - m_h(d_{n_2} - c_h \sin(\Omega_0 t)^2))\dot{U}_8 \\
&\quad - d_{n_2}(\overline{F}^d_{1_0} - \overline{F}^u_{1_0})\cos(\Omega_0 t) - (I_{s_{\text{lat}}} + I_{y1} + m_s c_s^2 + m_y c_n^2 + I_{h_3}\sin(\Omega_0 t)^2 \\
&\quad - (d_{h_1} - d_{n_2})\sin(\Omega_0 t)\hat{F}^d_{2_0} - (K_h - c_h d_{n_2} m_h \Omega_0^2)\cos(\Omega_0 t)q_h - \sin(\Omega_0 t)\hat{M}^d_{1_0} \\
&\quad - 2\Omega_0(I_{h_3} + c_h m_h(c_h - 1{\cdot}5d_{n_2}))\sin(\Omega_0 t)\cos(\Omega_0 t)U_3 - (C_h\cos(\Omega_0 t) \\
&\quad + \Omega_0(I_{h_2} - I_{h_1} - I_{h_3} - 2c_h m_h(c_h - d_{n_2}))\sin(\Omega_0 t))U_2 - c_h m_h \sin(\Omega_0 t)\cos(\Omega_0 t)\dot{U}_6 \\
&\quad + m_h(d_{n_2}^2 + c_h(c_h - 2d_{n_2})\sin(\Omega_0 t)^2))\dot{U}_3 - (I_{h_3} + c_h m_h(c_h - 2d_{n_2}))\sin(\Omega_0 t)\cos(\Omega_0 t)\dot{U}_1 \\
0 &= \hat{M}^d_{3_0} + \hat{M}^t_{2_l} + \hat{M}^u_{3_0} + d_{h_2}\hat{F}^d_{2_0} + d_{h_2}\hat{F}^u_{2_0} - d_{n_2}(\overline{F}^d_{1_0} - \overline{F}^u_{1_0})\cos(\Omega_0 t)q_y - (I_{h_2} + I_{s_{\text{long}}} + I_{y2})\dot{U}_4 \\
0 &= \hat{M}^t_{3_l} + K_y q_y \\
0 &= \hat{F}^t_{1_l} + \sin(\Omega_0 t)\hat{F}^u_{1_0} + \cos(\Omega_0 t)\hat{F}^u_{2_0} + 2c_h m_h \Omega_0 \cos(\Omega_0 t)U_2 + c_h m_h \Omega_0^2 \sin(\Omega_0 t)q_h \\
&\quad + 3c_h m_h \Omega_0 \sin(\Omega_0 t)\cos(\Omega_0 t)U_1 + c_h m_h \sin(\Omega_0 t)\dot{U}_2 - (\overline{F}^d_{1_0} - \overline{F}^u_{1_0})\sin(\Omega_0 t) \\
&\quad - \sin(\Omega_0 t)\hat{F}^d_{1_0} - \cos(\Omega_0 t)\hat{F}^d_{2_0} - 2c_h m_h \Omega_0(1 - 1{\cdot}5\sin(\Omega_0 t)^2)U_3 - (m_h + m_s + m_y)\dot{U}_6 \\
&\quad - c_h m_h \sin(\Omega_0 t)\cos(\Omega_0 t)\dot{U}_3 - (c_n m_y + c_s m_s - m_h(d_{n_2} - c_h\cos(\Omega_0 t)^2))\dot{U}_1 \\
0 &= \hat{F}^d_{3_0} + \hat{F}^t_{2_l} + \hat{F}^u_{3_0} - (\overline{F}^d_{1_0} - \overline{F}^u_{1_0})q_h - (\overline{F}^d_{1_0} - \overline{F}^u_{1_0})\sin(\Omega_0 t)q_y - (m_h + m_s + m_y)\dot{U}_7 \\
0 &= \hat{F}^t_{3_l} + \sin(\Omega_0 t)\hat{F}^d_{2_0} + \cos(\Omega_0 t)\hat{F}^u_{1_0} + c_h m_h \Omega_0^2 \cos(\Omega_0 t)q_h - (m_h + m_s + m_y)\dot{U}_8 \\
&\quad + 3c_h m_h \Omega_0 \sin(\Omega_0 t)\cos(\Omega_0 t)U_3 + c_h m_h \cos(\Omega_0 t)\dot{U}_2 + c_h m_h \sin(\Omega_0 t)\cos(\Omega_0 t)\dot{U}_1 \\
&\quad + (c_n m_y + c_s m_s - m_h(d_{n_2} - c_h \sin(\Omega_0 t)^2))\dot{U}_3 - (\overline{F}^d_{1_0} - \overline{F}^u_{1_0})\cos(\Omega_0 t) - \sin(\Omega_0 t)\hat{F}^u_{2_0} \\
&\quad - \cos(\Omega_0 t)\hat{F}^d_{1_0} - 2c_h m_h \Omega_0 \sin(\Omega_0 t)U_2 - c_h m_h \Omega_0(-1 + 3\sin(\Omega_0 t)^2)U_1
\end{aligned}
$$

where Ω_0 is the nominal shaft angular speed; c_n, c_s, c_h are, respectively, distances from the yaw axis to the nacelle mass center, from the yaw axis to the shaft mass center, and from the teeter axis to the hub mass center; d_{n_2} is the distance from the yaw axis to the teeter axis; d_{h_1} is the distance from the shaft axis to the blade root; d_{h_2} is the distance from the teeter axis to the blade root; I_{y_1}, I_{y_1}, and I_{y_1} are the moments of inertia of the nacelle about axes fixed in the nacelle; and $I_{s_{\text{long}}}, I_{s_{\text{lat}}}$ are the moments of inertia of the shaft about the longitudinal and lateral axes; I_{h_1}, I_{h_1}, and I_{h_1} are the moments of inertia of the hub about axes fixed in the hub; $\hat{F}^u_{1_0}, \hat{F}^u_{2_0}$, and $\hat{F}^u_{3_0}$ denote the forces on the hub transferred from the blade U at the point of attachment (root); $\hat{M}^u_{1_0}, \hat{M}^u_{2_0}$, and $\hat{M}^u_{3_0}$ denote the corresponding moments, and $\hat{F}^d_{1_0}, \hat{F}^d_{2_0}, \hat{F}^d_{3_0}, \hat{M}^d_{1_0}, \hat{M}^d_{2_0}$, and $\hat{M}^d_{3_0}$ are the forces and moments transferred by the blade D; $\overline{F}^u_{1_0}$ and $\overline{F}^d_{1_0}$ are the steady-state axial forces of each blade; and $\hat{F}^t_{1_l}, \hat{F}^t_{2_l}, \hat{F}^t_{3_l}, \hat{M}^t_{1_l}, \hat{M}^t_{2_l}$, and $\hat{M}^t_{3_l}$ denote the forces and moments transferred by the tower.

References

1. Quarton DC, Rasmussen F, Nath C, Argyriadis K. Wind turbine design calculation—the state of the art. *Proceedings of the European Union Wind Energy Conference, Göteborg*, 1996; 10–15.
2. Garrad AD. Dynamics of wind turbines. *IEEE Proceedings* 1983; **130**(9): 523–530.
3. Molenaar D, Dijkstra S. State-of-the-art of wind turbine design codes: main features overview for cost-effective generation. *Wind Engineering* 1999; **23**(5): 295–311.

4. Bauchau OA, Bottasso CL, Nikishkov YG. Modeling rotorcraft dynamics with finite element multibody procedures. *Mathematical and Computer Modeling* 2001; **33**: 1113–1137.
5. Hodges DH, Patil MJ. Multi-flexible-body analysis for application to wind-turbine control design. *AIAA Paper 2000-0030*, 2000.
6. Kane TR, Levinson DA. *Dynamics: Theory and Applications*. McGraw-Hill: New York, 1985.
7. Hodges DH. A mixed variational formulation based on exact intrinsic equations for dynamics of moving beams. *International Journal of Solids and Structures* 1990; **26**(11): 1253–1273.
8. Borri M, Mantegazza P. Some contributions on structural and dynamic modeling of helicopter rotor blades. *L'Aerotecnica Missili e Spazio* 1985; **64**(9): 143–154.
9. Simo JC, Vu-Quoc L. On the dynamics in space of rods undergoing large motions—a geometrically exact approach. *Computer Methods in Applied Mechanics and Engineering* 1988; **66**: 125–161.
10. Bauchau OA, Kang NK. A multibody formulation for helicopter structural dynamic analysis. *Journal of the American Helicopter Society* 1993; **38**(2): 3–14.
11. Reissner E. On one-dimensional large-displacement finite-strain beam theory. *Studies in Applied Mathematics* 1973; **LII**(2): 87–95.
12. Cesnik CES, Hodges DH. VABS: a new concept for composite rotor blade cross-sectional modeling. *Journal of the American Helicopter Society* 1997; **42**(1): 27–38.
13. Borri M. Helicopter rotor dynamics by finite element time approximation. *Computers and Mathematics with Applications* 1986; **12A**: 149–160.
14. Peters DA. Fast Floquet theory and trim for multi-bladed rotorcraft. *Journal of the American Helicopter Society* 1994; **39**(4): 82–89.
15. Hodges DH, Shang X, Cesnik CES. Finite element solution of nonlinear intrinsic equations for curved composite beams. *Journal of the American Helicopter Society* 1996; **41**(4): 313–321.
16. Patil MJ, Hodges DH, Cesnik CES. Nonlinear aeroelastic analysis of complete aircraft in subsonic flow. *Journal of Aircraft* 2000; **37**(5): 753–760.
17. Peters DA, Boyd DD, He C-J. Finite-state induced-flow model for rotors in hover and forward flight. *Journal of the American Helicopter Society* 1989; **34**(4): 5–17.
18. Shang X, Hodges DH, Peters DA. Aeroelastic stability of composite hingeless rotors in hover with finite-state unsteady aerodynamics. *Journal of the American Helicopter Society* 1999; **44**(3): 206–221.
19. Mitiguy PC, Kane TR. Motion variables leading to efficient equations of motion. *International Journal of Robotics Research*. 1996; **15**(5): 522–532.

